Evaluation of the daytime tropospheric loss of 2-methylbutanal

María Asensio[1,2], María Antiñolo[1,2,†], Sergio Blázquez[2], José Albaladejo[1,2], Elena Jiménez[1,2,*]

[1]Instituto de Investigación en Combustión y Contaminación Atmosférica, Universidad de Castilla-La Mancha, Camino de Moledores s/n, Ciudad Real, 13071, Spain

5 [2]Departamento de Química Física, Universidad de Castilla-La Mancha, Avda. Camilo José Cela 1B, Ciudad Real, 13071, Spain

Correspondence to: Elena Jiménez (elena.jimenez@uclm.es)

Abstract. Saturated aldehydes, *e.g.* 2-methylbutanal (2MB, $CH_3CH_2CH(CH_3)C(O)H$), are emitted into the atmosphere by several biogenic sources. The first step in the daytime atmospheric degradation of 2MB involves gas-phase reactions initiated

10 by hydroxyl (OH) radicals, chlorine (Cl) atoms and/or sunlight. In this work, we report the rate coefficients for the gas-phase reaction of 2MB with OH (k_{OH}) and Cl (k_{Cl}) together with the photolysis rate coefficient (J) in the ultraviolet solar actinic region in Valencia (Spain) at different times of the day. The temperature dependence of k_{OH} was described in the 263-353 K range by the following Arrhenius expression: $k_{OH}(T)=(8.88\pm0.41)\times10^{-12} \exp[(331\pm14)/T]$ cm^3 molecule^{-1} s^{-1}. At 298 K, the reported k_{OH} and k_{Cl} are $(2.68\pm0.07)\times10^{-11}$ cm^3 molecule^{-1} s^{-1} and $(2.16\pm0.32)\times10^{-10}$ cm^3 molecule^{-1} s^{-1}, respectively.

15 Identification and quantification of the gaseous products of the Cl-reaction and those from the photodissociation of 2MB were carried out in a smog chamber by different techniques (Fourier transform infrared spectroscopy, proton transfer time-of-flight mass spectrometry, and gas chromatography coupled to mass spectrometry). The formation and size distribution of secondary organic aerosols formed in the Cl-reaction was monitored by a fast mobility particle sizer spectrometer. A discussion on the relative importance of the first step in the daytime atmospheric degradation of 2MB is presented together with the impact of

20 the degradation products in marine atmospheres.

1 Introduction

The saturated aldehyde 2-methylbutanal (2MB, $CH_3CH_2CH(CH_3)C(O)H$) is emitted into the low atmosphere from several sources. It is known that 2MB is formed during the fermentation and drying processes of cocoa beans (Utrilla-Vázquez et al., 2020), the manufacturing process of tea leaves (*e.g.* Camellia Sinensis (Flaig et al., 2020)), and as a consequence of the stress

25 suffered by grapevine leaves due to drought (Griesser et al., 2015). Besides, this aldehyde is emitted into the atmosphere by wildland fires (Urbanski et al., 2008) and many industrial activities, such as poultry rendering operations when animal by-products are processed (Kolar and Kastner, 2010). As a secondary pollutant, 2MB can be formed in situ in the atmosphere by oxidation of 2-methyl-1-butanol ($CH_3CH_2CH(CH_3)CH_2OH$), which is used as a biochemical pesticide, commercially used as a solvent in paints and oils and as flavorant in many processed foods.

30 Once in the atmosphere, 2MB can react with daytime tropospheric oxidants, such as hydroxyl (OH) radicals or chlorine atoms (Cl) in coastal or marine regions. During daytime, 2MB can also be photolyzed by the solar actinic radiation ($\lambda>290$ nm). Other possible sinks of 2MB are dry and wet deposition, that have been previously reported to be minor sinks for other aldehydes such as acetaldehyde (Millet et al., 2010). Since the gas-phase chemistry of 2MB can lead to the formation of secondary pollutants, its emission may have a significant impact on tropospheric chemistry and air pollution at a local/regional

35 scale. For that reason, in this work we evaluate the potential impact of the diurnal degradation of 2MB. Firstly, the photodissociation of 2MB (Reaction R1) has been investigated at room temperature by determining its absorption cross

---

† Currently at *Escuela de Ingeniería Industrial y Aeroespacial*. Universidad de Castilla-La Mancha. Avenida Carlos III s/n. Real Fábrica de Armas. 45071 Toledo (Spain).

sections (σ_λ) between 220 and 360 nm, the photolysis rate coefficient (J) under the irradiation conditions of this work ($\lambda \geq 290$ nm) and the corresponding effective quantum yield (ϕ_{eff}).

$$CH_3CH_2CH(CH_3)C(O)H + h\nu\ (\lambda \geq 290\ nm) \rightarrow Products \qquad J \qquad\qquad (R1)$$

Secondly, the gas-phase kinetics with OH (Reaction R2) and Cl (Reaction R3) under tropospheric conditions of temperature and pressure was investigated to assess the tropospheric lifetime (τ) of 2MB due to both removal routes.

$$OH + CH_3CH_2CH(CH_3)C(O)H \rightarrow Products \qquad k_{OH} \qquad\qquad (R2)$$

$$Cl + CH_3CH_2CH(CH_3)C(O)H \rightarrow Products \qquad k_{Cl} \qquad\qquad (R3)$$

The rate coefficient k_{OH} was determined between 263 and 353 K as a function of total pressure (50-600 Torr of He), while k_{Cl} was measured at 298 K and (760±5) Torr of air. Finally, the gaseous products of reactions R1 and R3 have been identified under NO$_x$-free conditions using several detection techniques and a reaction mechanism is proposed for NOx-free atmosphere. Furthermore, the formation yield of secondary organic aerosols (SOAs) formed in reaction R3 has been measured to assess the impact of 2MB on the formation of ultrafine particles. With all this information, we discuss the potential impact of atmospheric 2MB on local or regional air quality in terms of the estimated tropospheric lifetime and the reaction products formed.

2 Experimental methods

In this section, a brief description of the experimental techniques and the methodology employed in this work is given. More details can be found in the Supporting Information (SI).

2.1 Photodissociation of 2-methylbutanal

2.1.1 Gas-phase ultraviolet (UV) absorption spectroscopy (220-360 nm)

Ultraviolet absorption spectroscopy was used to determine the absorption cross sections of 2MB as a function of wavelength (σ_λ in base e) between 220 and 360 nm. The experimental setup employed in this work has been described in detail elsewhere (Blázquez et al., 2020). This system consists of a deuterium-tungsten light source (DT-200, StellarNet) placed at the entrance of a 107.15 cm jacketed Pyrex® cell, connected by an optical fibre to a f/2 spectrometer that possesses a concave holographic grating (590 grooves/mm) and a 2048-pixels CCD camera (BLACK-Comet model C, StellarNet). The absorbance is recorded in a computer with the data acquisition software (SpectraWiz v5.33). The experiments were carried out by introducing pure gaseous 2MB (1.085 – 6.642 Torr) into the UV cell in static mode. Applying the Beer-Lambert's law, σ_λ was determined from the slope of the absorbance (in base e) versus 2MB concentration ([2MB]). **Figure S1** of the SI shows some examples of the absorbance *versus* [2MB]. Even though the spectral resolution of the recorded UV spectra was higher than 0.11 nm, in **Table S1** absolute values of σ_λ are only given at 1-nm intervals for ease of presentation. Note that the tabulated values are not the integrated σ_λ in 1 nm. All absolute σ_λ are available in the Excel file included as SI.

2.1.2 Continuous irradiation with a solar simulator ($\lambda \geq 290$ nm)

A schematic of the set-up used in this work to investigate the photochemistry of 2MB under atmospheric conditions is shown in **Fig. 1**. A Pyrex (l=20 cm and ϕ=4 cm) cell sealed with quartz windows was filled with (760 ± 3) Torr of diluted 2MB (interval of dilution factor from 6.96×10^{-4} to 1.92×10^{-3} in synthetic air) from a 10-L Pyrex storage bulb at (298 ± 2) K. The partial pressure of 2MB, the total pressure inside the storage bulb and the pressure in the photolysis cell were measured by capacitance pressure transducers (Leybold, model Ceravac, 10 and 1000 Torr full scale). The initial concentration of 2MB in the photolysis cell ranged from 1.2 to 6.9×10^{16} molecules cm^{-3}, measured by FTIR spectroscopy. Before irradiating the sample

75 and after each irradiation time, the Fourier transform infrared (FTIR) spectrum of the mixture was recorded in a 16-L White-type cell with an optical path length of 96 m by a FTIR spectrometer (Thermo Fischer Scientific, model Nicolet Nexus 870) with a liquid N_2-cooled MCT (Mercury Cadmium Telluride) detector. IR spectra were recorded between 650 and 4000 cm^{-1} at a resolution of 2 cm^{-1}, after the accumulation of 32 interferograms. The selected IR bands for monitoring 2MB were the ones centered at 2700 and 2800 cm^{-1}.

80 The sample of 2MB in air was irradiated by an ABA class solar simulator (SunLite^{TM} Solar Simulator, model 11002-2) during 30, 60, 90, 120, and 150 min. The solar simulator, equipped with a Xe arc lamp and an Air Mass (AM) 1.5G filter, emits radiation over 290 nm with a spectrum that simulates the solar reference spectrum AM 1.5G (see **Fig. S2** of the SI). This reference spectrum corresponds to the terrestrial solar spectral irradiance at the surface when the air mass factor is 1.5 and the sun is about 41° above the horizon and under specific atmospheric conditions defined by the U.S. Standard Atmosphere

85 (Gueymard et al., 2002). Irradiance was determined in each experiment with a 1-cm^2 solar reference cell for which a 100 mV output corresponds to 1 Sun, defined as the irradiance of the AM1.5G reference solar spectrum described above. In this work, the measured irradiance was (2.225±0.145) Suns.

As shown in **Fig. 1**, during the irradiation of the diluted sample of 2MB, control valves 2 and 3 were closed. After irradiation, the gas sample was expanded to the 16-L FTIR cell to measure the 2MB concentration over time ([2MB]$_t$) and, thus, to

90 determine the photolysis rate coefficient, J. In that case, the total pressure decreases to 7 Torr and control valves 1 and 4 were closed.
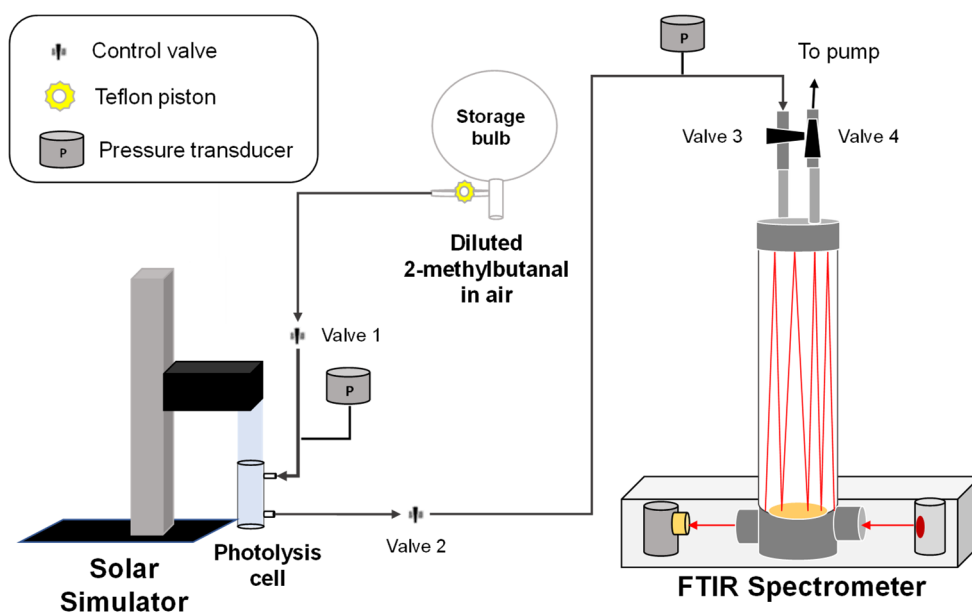
Figure 1. Schematics of the photolysis set-up using a solar simulator as a continuous irradiation source:

95

Possible losses due to the heterogeneous reaction of 2MB onto the walls were evaluated in experiments without light at different times (45, 90 and 135 min). As the photolysis cell used has a large surface/volume ratio (276.46 cm^2/251.33 cm^3= 1.1 cm^{-1}), the heterogeneous loss of 2MB contributes significantly to the total decay of 2MB. The heterogeneous loss rate, $k_{heterog}$ (in s^{-1}), has been measured to contribute around 24% to the total loss. Therefore, the photolysis rate coefficient of 2-

100 methylbutanal at $\lambda > 290$ nm, J (in s^{-1}), can be obtained from the slope of the plot of $ln([2MB]_0/[2MB]_t)$ versus time according to Eq. (1).

$$ln([2MB]_0/[2MB]_t) = (k_{heterog}+J)t \qquad (1)$$

For the identification of the photolysis products, three complementary detection techniques were used: FTIR spectroscopy, gas chromatography-mass spectrometry (GC-MS) and proton transfer reaction time-of-flight mass spectrometry (PTR-ToF-

MS). The gas chromatography-mass spectrometer (Thermo Electron, models Trace GC Ultra and DSQ II) was equipped with a BPX35 column (30 m × 0.25 mm ID × 0.25 μm, SGE Analytical Science) working at a temperature ramp that ranged between 40 and 250 °C (Ballesteros et al., 2017). The solid-phase microextraction technique was used as a sampling method in these experiments, thus, a 50/30 μm divinylbenzene/carboxen/polydimethylsiloxane (DVB/CAR/PDMS) fibre (Supelco) was exposed during 10 min to the gas mixture of the photolysis cell and then, the fibre was injected into the GC-MS during 5 min.

Independently, in some experiments a PTR-ToF-MS (IONICON, model PTR-TOF 4000), working with a field density ratio (E/N) of 137 Td, a time resolution of 20 s, and a detected mass range between 29 and 390.86 a.m.u. (Antiñolo et al., 2010) was coupled to the FTIR cell, in which the content of the photolysis cell was diluted in 760 Torr of air, to detect the photolysis products at the end of the experiment. However, quantification of the photolysis products could only be carried out by FTIR spectroscopy. The PTR-ToF-MS could not be used to quantify them as the sampling flow rate was too high, making the total pressure in the FTIR cell drop rapidly and it did not allow for a stable signal. The quantification by GC-MS was not performed due to the absence of an internal standard that would have been needed due to the instability of the GC-MS signal.

2.2 Pulsed laser photolysis coupled to laser induced fluorescence (PLP-LIF) technique

The absolute kinetic study of the reaction of OH radicals with 2MB (reaction R2) was performed as a function of temperature (T = 263-353 K) and total pressure (P_T = 50-600 Torr of He) in a Pyrex doubled-wall reactor of $ca.$ 200 mL (Martínez et al., 1999). The gas temperature was measured by a type K (chromel–alumel) thermocouple inserted several millimetres above the reaction and T was kept constant (±0.2 K) during each experiment. The total pressure inside the reactor was controlled by a needle valve placed at the exit of the reactor and prior to the pump and it was measured by pressure transducers (Oerlikon Leybold Vacuum, model CERAVAC CTR 100N, 0-100 Torr and 0-1000 Torr). All gases were introduced in the reactor by means of mass flow controllers. The total flow through the reactor, F_{Total}, was kept constant in the 485-496 sccm range, while the flow rate of diluted 2MB and OH-precursor (H_2O_2 or HNO_3) were varied between 3.1 and 29 standard cubic centimetre, sccm) and between 14.4 and 96.8 sccm, respectively. The residence time in the cell ranged between 0.8 and 13 s, depending on the total flow, pressure, and temperature conditions of the experiment. More details are given in the SI.

The OH radicals were generated in $situ$ from the pulsed laser photolysis (PLP) of H_2O_2 or HNO_3 at 248 nm, radiation coming from a KrF excimer laser (Coherent, ExciStar 200). The laser fluence was 23 mJ pulse^{-1} cm^{-2} at 10 Hz. The OH radicals generated in the electronic ground state were excited at $ca.$ 282 nm (laser energy between 0.4 and 1.0 mJ pulse^{-1} at 10 Hz) to the first excited electronic state by a tuneable pulsed laser (Continuum, ND60; pumped by Continuum, NY 81 CA-10). The photolysis and excitation lasers traverse the reactor perpendicularly. From the intersection of both lasers, in which reaction takes place, the excited OH radicals emit off-resonance laser induced fluorescence (LIF) (at $ca.$ 310 nm), which was collected by a photomultiplier tube (Thorn EMI, 9813B model) set perpendicular to both lasers.

Under $pseudo$-first order conditions ($i.e.,$ when the initial concentration of OH-precursor and 2MB are in large excess with respect to that of OH radicals), the time evolution of the LIF signal follows a single exponential decay (see some examples in **Fig. S3**). From the analysis of these decays, the $pseudo$-first order rate coefficient, k', was determined at given [OH-precursor]$_0$ and [2MB]$_0$ for each temperature and pressure. In the absence of 2MB, the measured $pseudo$-first order rate coefficient is k_0'.

Examples of the k'-k'_0 $versus$ [2MB]$_0$ plots at 263 and 353 K, from which the rate coefficient k_{OH} was obtained, are depicted in **Fig. S4**. [OH-precursor]$_0$ was measured by UV absorption spectroscopy between 200 and 230 nm using the same experimental system described in Sect. 2.1.1. In this case, the absorption measurements were carried out under flowing conditions. From [OH-precursor]$_0$ and the laser fluence at 248 nm, the initial amount of OH radicals inside the reactor cell was estimated. The ranges of [OH-precursor]$_0$, [2MB]$_0$, dilution factor f of 2MB in the storage bulb, and k' are also listed for each temperature and pressure in **Table S2** of the SI.

2.3. Simulation (*smog*) chambers coupled to a variety of detection techniques

For the kinetic and mechanistic study of the Cl-reaction with 2MB, several experimental systems were used (Ballesteros et al., 2017; Antiñolo et al., 2019; Antiñolo et al., 2020). Two cylindrical chambers made of Pyrex were available to perform the different experiments: a 16-L cell and 264-L reactor. Both chambers were surrounded by actinic lamps (Philips Actinic BL TL 40W/10 1SL/25, λ= 340–400 nm): four for the 16-L gas cell and eight for the 264-L. These lamps were used to continuously generate Cl atoms *in situ* by UV photolysis of Cl_2. The gas-phase species (2MB and Cl_2) were introduced in the reactor from a gas-line, and they were diluted with synthetic air at (298±2) K and (760±5) Torr of total pressure. The total pressure in the gas-line and in the reactors was measured with two capacitor pressure transducers (Leybold, model Ceravac, 10- and 1000-Torr full scale). Three different detection methods were employed: FTIR spectroscopy, GC-MS and PTR-ToF-MS, previously described in Sect. 2.1.2.

2.3.1. Relative rate kinetic studies (298 K and 760 Torr of air)

The kinetic experiments were carried out by mixing 2MB, a reference compound (ethanol or isoprene), Cl_2, and synthetic air in the 16-L cell and using FTIR to monitor 2MB and the reference compound as a function of reaction time. The IR bands selected for monitoring the loss of 2MB and the reference compounds were centred at 2700 cm^{-1} for 2MB, 1070 cm^{-1} for ethanol and 3095 cm^{-1} for isoprene. The disappearance of 2MB and the reference compound is mainly due to reaction with Cl, although they can also be lost by heterogeneous reaction onto the reactor walls, UV photolysis and/or reaction with the oxidant precursor. These loss processes were evaluated in preliminary and independent experiments in the absence of Cl_2 and UV light (wall loss, k_w), in the absence of UV light (reaction with Cl_2, $k'_{Cl_2} = k_{Cl_2}[Cl_2]_0$) and irradiating in the absence of Cl_2 (UV photolysis, k_{hv}) as described in previous studies (Antiñolo et al., 2019; Antiñolo et al., 2020). **Table 1** summarizes the loss rate coefficients for these processes and the overall loss rate coefficients, k_{Total_loss} (k_{loss} for 2MB and $k_{Ref,loss}$ for the reference compound).

Table 1. Measured loss rate coefficients of 2MB and the reference compounds.

Compound	k_w (10^{-4} s^{-1})	k'_{Cl_2} (10^{-5} s^{-1})	k_{hv} (10^{-5} s^{-1})	k_{Total_loss} (10^{-4} s^{-1})
2MB	3.20 ± 1.15	negl.	negl.	3.20 ± 1.15
Ethanol	10.7 ± 0.14	negl.	negl.	10.7 ± 0.14
Isoprene	2.27 ± 0.99	9.54 ± 0.54	negl.	11.8 ± 1.13

negl.: negligible

Therefore, taking into account the overall losses for both 2MB and the reference compound, the integrated rate equation is given by the following expression:

$$\ln\left(\frac{[2MB]_0}{[2MB]_t}\right) - k_{loss}t = \frac{k_{Cl}}{k_{ref}}\left[\ln\left(\frac{[Ref]_0}{[Ref]_t}\right) - k_{Ref,loss}t\right] \tag{2}$$

where k_{ref} is the rate coefficient for the Cl-reaction with the reference compound at 298 K and 760 Torr. $[2MB]_0$, $[2MB]_t$, $[Ref]_0$ and $[Ref]_t$ are the concentrations of 2MB and the reference compound at the beginning of the reaction and at a reaction time t, respectively. Initial concentrations in the cell were $[2MB]_0 = (4.9 - 6.6) \times 10^{14}$ molecules cm^{-3}, $[Cl_2]_0 = (3.3 - 5.9) \times 10^{14}$ molecules cm^{-3}, $[ethanol]_0 = (4.6 - 3.6) \times 10^{14}$ molecules cm^{-3} and $[isoprene]_0 = (5.1 - 5.7) \times 10^{14}$ molecules cm^{-3}. In **Fig. S5**, an example of the plots of Eq. (2) is presented for both reference compounds.

2.3.2. Product study in the Cl reaction

The identification of the gaseous products generated in the reaction of 2-methylbutanal with Cl atoms was performed using complementary detection techniques: FTIR spectroscopy (using the 16-L reactor) (Ballesteros et al., 2017; Antiñolo et al., 2019), GC-MS, and PTR-ToF-MS (using the 264-L simulation chamber) (Antiñolo et al., 2020) in separate experiments. In all cases, preliminary tests were carried out to check if products were generated during the dark reaction of 2MB with Cl_2 and/or during the UV light exposure of 2MB. When GC-MS was used, no products due to these processes were observed. Nevertheless, with FTIR and PTR-ToF-MS the formation of some products was observed during UV light exposure of 2MB (see Sect. 4.3.1). In all the experiments, synthetic air was used as diluent gas at 298 K and 760 Torr, and the reaction mixture was irradiated for 60 min. IR spectra, chromatograms, and mass spectra were recorded every 2 min, 10 min and 20 sec respectively. In **Table 2**, the initial concentrations of 2MB/Cl_2/air mixtures are summarized. Because of the high sensitivity of the PTR-ToF-MS, the initial concentrations of 2MB and Cl_2 were reduced with respect to those employed in the FTIR and GC-MS experiments. Furthermore, at the inlet of the PTR-ToF-MS the reaction mixture was diluted (a factor of 1/5) with an air flow by means of a dynamic inlet dilution system to avoid signal saturation. Quantified products were corrected to account for their loss due to Cl reaction according to the method described by Ceacero-Vega et al. (2012).

Table 2. Initial concentrations of 2MB and Cl-precursor in the reactor.

Detection method	$[2MB]_0$ (10^{14} molecules cm^{-3})	$[Cl_2]_0$ (10^{14} molecules cm^{-3})
FTIR	3.6–6.2	2.2-12
GC-MS	6.2-8.8	6.5-8.5
PTR-ToF-MS	0.18-0.29	0.24-0.27

In addition to the gaseous reaction products, the secondary organic aerosols produced in the Cl+2MB reaction were detected and the size distribution of these SOAs was measured by a Fast Mobility Particle Sizer (FMPS) spectrometer (TSI 3091). The detailed experimental procedure can be found in the SI.

2.4. Chemicals

Gases: Synthetic air (99.999%, Air Liquide), Cl_2 (Sigma Aldrich, 99.8%), and He (Nippon Gases, 99.999%) were used as supplied. Liquids from Sigma Aldrich, with purities in brackets, were used after freeze-pump-thaw cycles: 2-methylbutanal (95%), ethanol (99.8%), isoprene (99%), butanone (99%), and acetaldehyde (99.5%). Aqueous solution of H_2O_2 (Sharlab, >50% v/v) was preconcentrated as described by Albaladejo et al. (2002).

3. Results and discussion

3.1 UV Photochemistry of 2-methylbutanal

3.1.1 Photolysis frequency (*J*) and effective quantum yield (Φ_{eff}) at $\lambda \geq 290$ nm

As shown in **Fig. 2**, 2MB absorbs in the ultraviolet range, exhibiting a weak absorption band in the 220-360 nm range, due to the forbidden n-π^* transition of the C=O chromophore, with a maximum at 296 nm. The maximum σ_λ was determined to be $(6.25 \pm 0.08) \times 10^{-20}$ cm^2 molecule^{-1} (stated uncertainty in our results throughout the document is $\pm 2\sigma$ statistical). Therefore, in the troposphere the actinic radiation ($\lambda \geq 290$ nm) can initiate photochemical processes for 2MB. Four photolysis experiments were performed under the conditions described in Sect. 2.1.2. In **Fig. 3** the average values of individual $ln([2MB]_0/[2MB]_t)$ obtained in the 4 experiments are plotted against t, showing a good linearity. From the slope of such a plot and correcting it with the wall losses of 2MB, as described in Sect. 2.1.2, $J = (1.96 \pm 0.32) \times 10^{-5}$ s^{-1} was obtained.

The photolysis quantum yield at a single wavelength (Φ_λ) is related to the photolysis rate coefficient as follows:

$$J = \int_{\lambda_1}^{\lambda_2} \Phi_\lambda \ \sigma_\lambda I_\lambda d\lambda \tag{4}$$

where I_λ is the irradiance in photons cm^{-2} nm^{-1} s^{-1} at λ. However, J can be approximated to:

$$J \cong \Phi_{\text{eff}} \sum_{\lambda_1}^{\lambda_2} I_\lambda \sigma_\lambda \Delta\lambda \qquad (5)$$

where, in this work, Φ_{eff} is the effective quantum yield of 2MB, $I_{\lambda>290\text{ nm}}$ is the measured irradiance at each wavelength, σ_λ is the experimentally determined UV absorption cross sections of 2MB, and $\Delta\lambda = 1$ nm. Taking into account all these parameters, $\Phi_{\text{eff}} = (0.30 \pm 0.05)$. An experiment was done in the presence of cyclohexane ([cyclohexane]/[2MB] = 8.2), which is widely used as OH-scavenger in this kind of experiment, to evaluate the impact of oxidants formed in this reaction. No difference was observed with the experiments with no cyclohexane, indicating that the chemistry of OH radical is negligible. This value is *ca.* half of that previously reported (Wenger, 2006) measured in the atmospheric simulation chamber EUPHORE (Valencia) under natural irradiation conditions, $\Phi_{\text{eff}} = (0.72 \pm 0.03)$. The reason for this difference is unknown. It is worth to note though that in the same study, for structurally similar aldehydes, like pentanal or 3-methylbutanal, the reported Φ_{eff} were closer ((0.30 ± 0.02), and (0.27 ± 0.01), respectively) to that determined in this work.
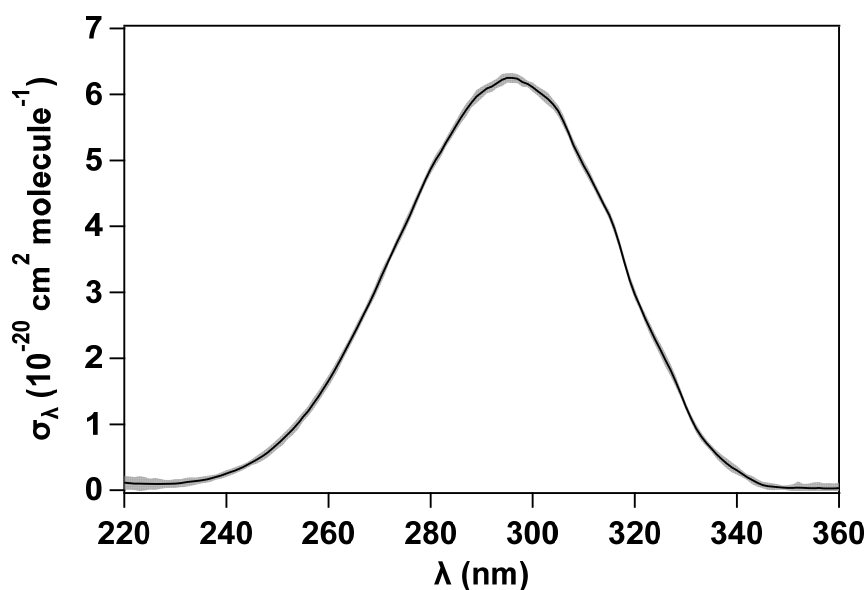
Figure 2. UV absorption cross sections of 2MB at 298 K. The grey shadow represents the statistical uncertainty.
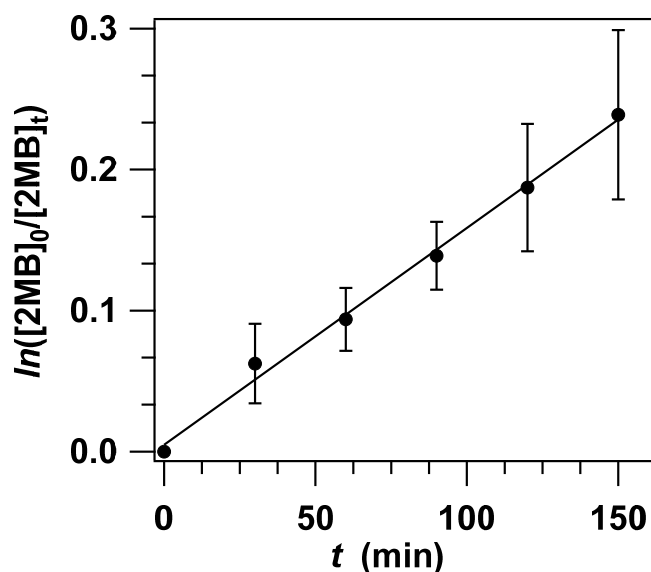
Figure 3. Plot of Eq. (1) in which the average $ln([2MB]_0/[2MB]_t)$ over time has been represented.

3.1.2. UV Photolysis products of 2MB

Photodissociation of 2MB by UV radiation can proceed through the following channels:

$$CH_3CH_2CH(CH_3)C(O)H + h\nu(\lambda \geq 290nm) \rightarrow CH_3CH_2CH(CH_3)C(O) + H \qquad (R1a)$$

$$\rightarrow CH_3CH_2CH(CH_3) + HC(O) \qquad (R1b)$$

$$\rightarrow CH_3CH_2CH_2CH_3 + CO \qquad (R1c)$$
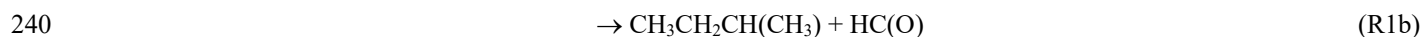
Channels (R1a) and (R1b) are radical-forming channels, while channel (R1c) yields close-shell molecules, i.e., butane ($CH_3CH_2CH_2CH_3$) and carbon monoxide (CO). **Figure 4a** shows the recorded IR spectra of the 2MB/air sample before irradiation. After 150 min of irradiation, the IR features from 2MB were subtracted to identify the formed products, as shown in **Fig. 4b**. Products from channel (R1c), butane and CO, were clearly identified at 2800 - 3000 cm^{-1} and 2000 - 2300 cm^{-1} respectively, indicating that this channel is open in the investigated wavelength range. The product yield ($Y_{product}$) is obtained from the slope of [Product] versus the consumed 2MB, Δ[2MB]. To determine the effective quantum yield of channel (R1c), ϕ_{1c}, the yield of formation of CO (Y_{CO}) or butane (Y_{butane}) could be used if no secondary chemistry was present, which is not the case for CO, since it is a very end degradation product and can be formed in many oxidation reactions. Therefore, CO is not a good marker for the importance of the photolysis channel R1c. In addition, Y_{CO} was observed to increase when the initial concentration of 2MB decreased. Butane was quantified using the reference spectra shown in **Fig. S6** and the (2800-3000) cm^{-1} IR band, yielding Y_{butane} = (9.80±0.31)% (see **Fig. S10**). As presented in **Fig. 4b**, butanone ($CH_3CH_2C(O)CH_3$) was also identified as a product of 2MB photolysis in the presence of air and its product yield was $Y_{butanone}$ = (14.8±0.5)% (see **Fig. S10**). Quantification of butanone was done using the reference spectra shown in **Fig. S6** for the IR bands: (2850-3100) cm^{-1} and (1650-1800) cm^{-1}. After subtracting the IR features of CO, butane and butanone, some IR features were left in the residual spectrum (**Figure 4c**). The band centered around 1040 cm^{-1} can be assigned to the C-O stretching mode of an alcohol (probably 2-butanol or methanol according to the proposed mechanism in Sect. 3.4.2) and the one centered around 1740 cm^{-1} can be assigned to the C=O stretching mode of a carbonyl group, alluding to aldehydes or ketones formation. The bands centered around 3000-2860 cm^{-1} can be assigned to the Csp^3-H stretching mode and finally, the bands located around 1300-1400 cm^{-1} can correspond to the C-H bending mode. However, the remaining IR bands in the residual spectrum could not be assigned to other gaseous oxidation products.
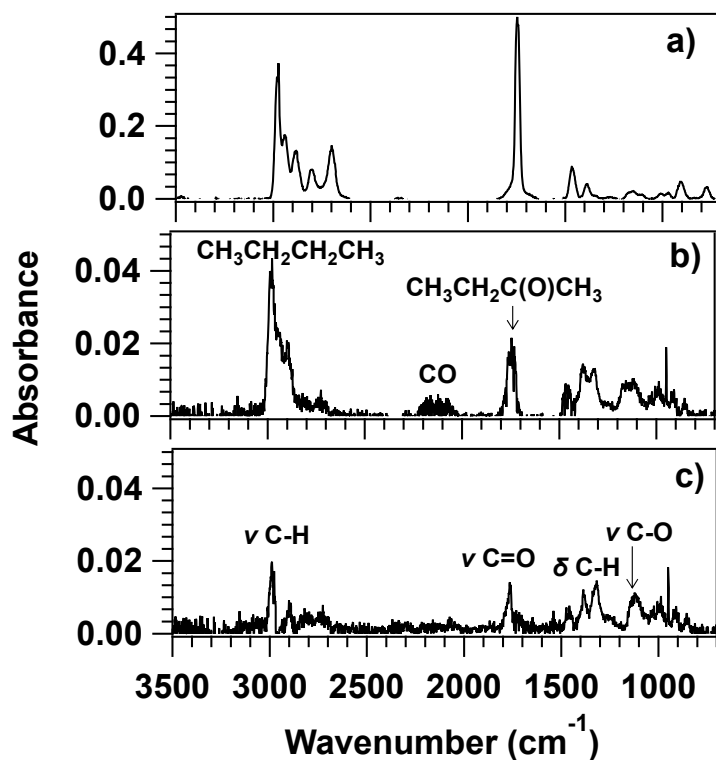
Figure 4. FTIR spectra of a 2-methylbutanal/air mixture (a) before irradiation; (b) after 150 min of photolysis with the features of 2MB subtracted (major products are labeled in the spectrum, exact positions of the bands are given in the main text) and (c) residual spectrum after the subtraction of the reference spectra of the identified products shown in Fig. S6.

Butanone was also identified by GC-MS and PTR-Tof-MS. **Figure S7** shows an example of the chromatogram of a mixture of 2MB in synthetic air, before and after photolysis (150 min). Although the PTR-ToF-MS technique allows the measurement of VOCs in gaseous samples as a function of time by taking some flow from the sample, the volume of the photolysis cell was too small to maintain the pressure during the photolysis experiments. For that reason, after 150 min of photolysis, the maximum photolysis time used in this work, the content of the photolysis cell was transferred to the 16-L chamber and diluted in synthetic air. This diluted sample was flowed through the PTR-Tof-MS during 5 min, in which mass spectra were measured. From the average of these mass spectra, only products could be detected but a temporal evolution could not be obtained. Under these conditions, butanone ($C_4H_8OH^+$, m/z = 73.06) was detected.

3.2 Kinetics of 2MB with OH at *T* and P-conditions of the troposphere

The individual rate coefficients for the 2MB+OH reaction obtained at a certain temperature and total cell pressure (P_T) are listed in **Table 3**. No pressure dependence of $k_{OH}(T)$ in the studied temperature range was observed, within the experimental uncertainties. For that reason, all $k'-k'_0$ values obtained at different total pressures were combined and plotted versus $[2MB]_0$, according to Eq. (ES3) of the SI, as shown in **Fig. S4** for 263 K and 353 K. The resulting $k_{OH}(T)$ are listed in the last column of **Table 3**. We observe a slight negative *T*-dependence of $k_{OH}(T)$, increasing 40 % from 353 K to 263 K. In **Fig. 5**, $k_{OH}(T)$ as a function of temperature is depicted, together with the previous reported data by D'Anna et al. (2001) at room temperature. The observed *T*-dependence is well-described by the following Arrhenius equation (solid line in **Fig. 5**):

$$k_{OH}(263\text{-}353 \text{ K}) = (8.88\pm0.81)\times10^{-12} \exp[(331\pm27)/ T] \text{ cm}^3 \text{ molecule}^{-1} \text{ s}^{-1} \tag{6}$$

where the activation energy is $-(2.75 \pm 0.23)$ kJ mol^{-1}. The reported k_{OH} by D'Anna et al. (2001) at room temperature was $(3.28\pm0.09)\times10^{-11}$ cm^3 molecule^{-1} s^{-1}, which is 22 % higher than the one obtained in this work, $k_{OH}(298 \text{ K}) = (2.68\pm0.07)\times10^{-}$

^{11} cm^3 molecule^{-1} s^{-1}. The reason for this discrepancy may be found in the different methods used: D'Anna et al. (2001) used a relative rate kinetic method with FTIR spectroscopy as detection technique in which they used air as bath gas at (298 ± 2) K and (760 ± 7) Torr. They only used one reference compound for their analysis, 1-butene, and that may result in an important source of error. In addition, the selected IR band for 1-butene (3140-3070 cm^{-1}) is too weak to be accurately monitored. Another possibility is that this band, or the selected one for 2MB (2740 – 2670 cm^{-1}), might interfere with IR features from reaction products.

Table 3. Individual rate coefficients of the 2MB + OH reaction as a function of temperature and total pressure.

T (K)	P_T (Torr)	$k_{OH}(T)$ (10^{-11} cm^3 molecule^{-1} s^{-1})	$k_{OH}(T)^*$ (10^{-11} cm^3 molecule^{-1} s^{-1})
263	50	3.15 ± 0.13	3.18 ± 0.10
	300	3.08 ± 0.15	
	600	3.31 ± 0.13	
268	50	3.03 ± 0.22	3.03 ± 0.17
	300	3.12 ± 0.15	
278	50	2.74 ± 0.16	2.87 ± 0.15
	300	3.02 ± 0.20	
	300	2.89 ± 0.24	
288	50	2.65 ± 0.22	2.78 ± 0.17
	300	2.84 ± 0.28	
	300	2.98 ± 0.17	
298	50	2.83 ± 0.12	2.68 ± 0.07
	50	2.76 ± 0.10	
	300	2.66 ± 0.11	
	600	2.62 ± 0.11	
309	50	2.68 ± 0.18	2.64 ± 0.13
	300	2.60 ± 0.15	
323	50	2.46 ± 0.10	2.46 ± 0.08
	300	2.46 ± 0.13	
338	50	2.38 ± 0.07	2.35 ± 0.06
	300	2.31 ± 0.10	
353	50	2.25 ± 0.09	2.27 ± 0.09
	300	2.40 ± 0.10	
	600	2.22 ± 0.07	

* Values obtained from the k'-k_0' versus [2MB]$_0$ plot combining all kinetic data at different total pressures
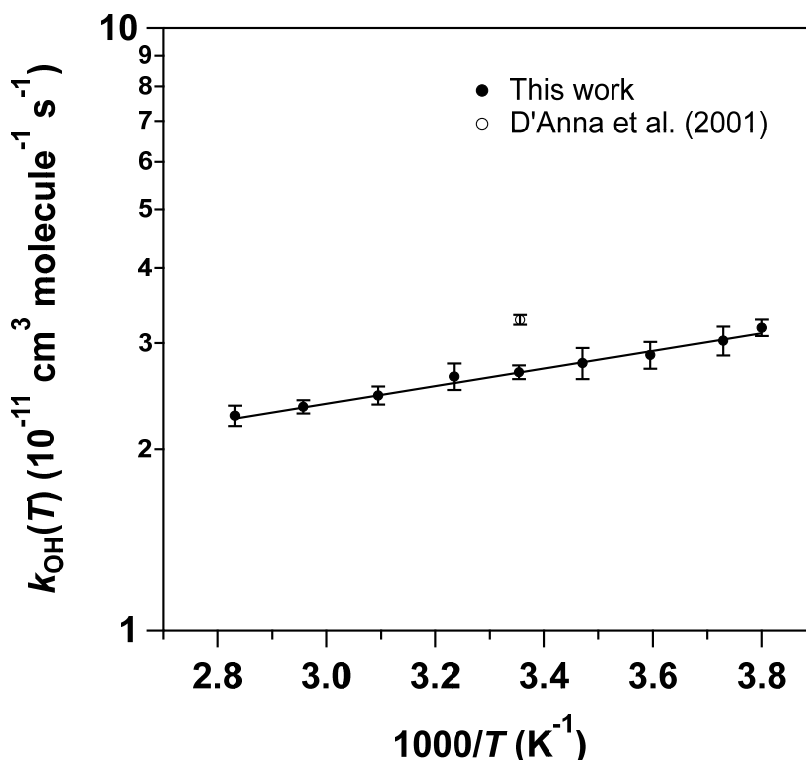
Figure 5. Arrhenius plot for the rate coefficient of the 2MB + OH reaction between 263 and 353 K.

3.3 Cl-reaction of 2MB at T and P-conditions of the marine boundary layer

3.3.1 Kinetics with Cl atoms

The plots of Eq. (2) for the two references used in this work can be seen in **Fig. S5**, in which a good linearity is shown, indicating that no secondary reactions were interfering. From the slope of these plots, k_{Cl}/k_{Ref} was obtained according to Eq. (2). Thus, from the rate coefficients of the reference compounds previously reported for the Cl-reaction of ethanol and isoprene (Atkinson et al., 2006; Orlando et al., 2003), k_{Cl} was determined. **Table 4** shows the rate coefficients obtained in this work with each reference compound and the averaged value, $(2.16 \pm 0.32) \times 10^{-10}$ cm³ molecule^{-1} s^{-1}. The uncertainty in k_{Cl} includes the propagation of the reported errors in k_{Ref}, the uncertainties in k_{loss} and the statistical errors from the slope of the plots shown in **Fig. S5**. The contribution of k_{loss} to the total loss of 2MB was found to be 4%.

Table 4. Results obtained in the kinetic experiments for the gas-phase reaction of Cl with 2-methylbutanal at 298 ± 2 K and 760 ± 5 Torr of air.

Reference	k_{Cl}/k_{Ref}	k_{Ref} (10^{-10} cm³ molecule^{-1} s^{-1})	k_{Cl} (10^{-10} cm³ molecule^{-1} s^{-1})
Ethanol	2.140 ± 0.038	1.00 ± 0.06 [1]	2.14 ± 0.27
Isoprene	0.509 ± 0.003	4.30 ± 0.58 [2]	2.19 ± 0.59
Average			**2.16 ± 0.32**

[1] Atkinson et al. (2006), [2] Orlando et al. (2003)

3.3.2 Identification and quantification of the gaseous products of the Cl + 2MB reaction

Identification by GC-MS: **Figure 6** shows the obtained chromatograms before and after 60 min reaction time and **Fig. S8** shows the mass spectra of the detected products corresponding to those chromatographic peaks. The peak corresponding to 2MB was observed at a retention time (RT) of 3.76 min. The rest of the peaks that appear in the chromatogram were assigned,

according to their mass spectrum, to the following products: acetaldehyde (RT = 2.15 min), 2-butanol (RT = 3.08 min), butanone (RT = 3.21 min), methylglyoxal (RT = 4.44 min), and 2-methylbutanoic acid (RT = 5.55 min).
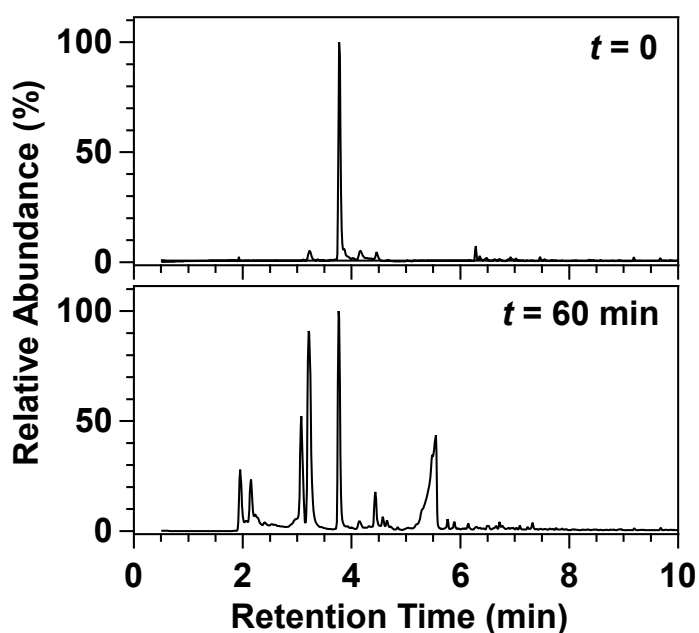
330   **Figure 6**. Chromatograms obtained for a 2MB/Cl_2 mixture before irradiation (top panel) and after 60 min of irradiation (bottom panel).

Identification and quantification by FTIR Spectroscopy: **Figure 7** shows the FTIR spectrum recorded after 50 min of reaction
335   time. The features of 2-methylbutanal have been subtracted for clarity purposes. By comparison with the reference spectra (shown in **Fig. S6**), the most abundant products observed were HCl, butanone, and CO. The yield for butanone, $Y_{butanone}$, obtained from the plots shown in **Fig. S9a**, was (53.1±1.6)%. Formation of acetaldehyde and formaldehyde was also observed, but their quantification was very imprecise due to the low signal of the residual spectrum, the similarity between both IR spectra and the possible presence of other minor products such as propanal and 2-butanol. After subtracting HCl, butanone,
340   and CO, ketene ($CH_2C(O)$) could be identified in the residual spectrum (shown in the bottom panel of **Fig. 7**) by comparison with the IR features reported by Wallington et al. (1996). The remaining bands could come from methylglyoxal, which was observed by GC-MS. It is worth noting that small amounts of acetaldehyde, formaldehyde, butanone and CO ($<9\times10^{12}$

molecules cm^{-3}) were observed during UV light exposure of 2-methylbutanal, but their amount was negligible compared with the observed ones during the Cl reaction (> 1 × 10^{14} molecules cm^{-3}).
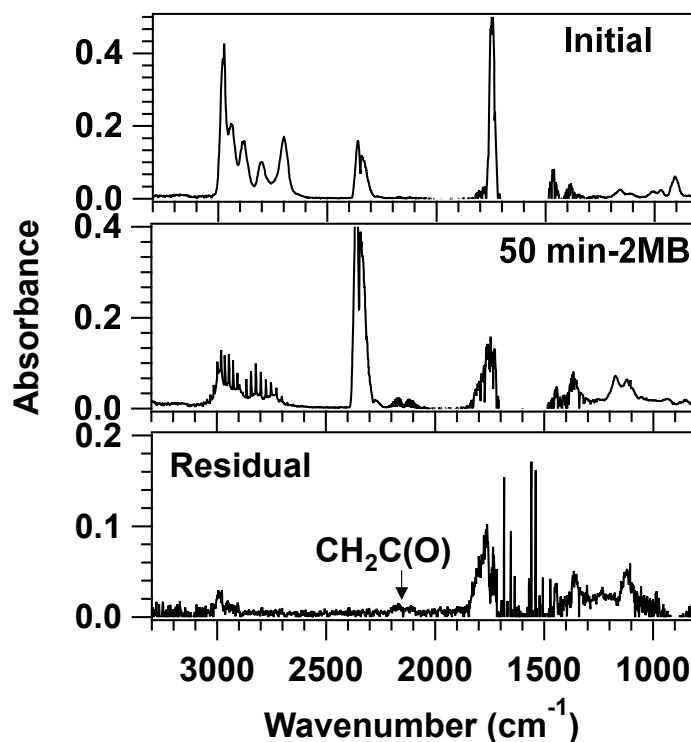
Figure 7. FTIR spectra used in the identification of the products in the Cl reaction of 2MB. The top panel shows the initial spectrum, the central panel shows the spectrum obtained after 50 min of Cl reaction, with the features of 2MB subtracted, and the bottom panel shows the residual spectrum after the subtraction of reaction products shown in the SI (**Figure S6**).

Identification by PTR-ToF-MS: The identified reaction products, with an average ion concentration greater than or equal to 0.2 ppb, were acetaldehyde (C$_2$H$_4$OH$^+$, *m/z* = 45.03), butanone (C$_4$H$_8$OH$^+$, *m/z* = 73.06), methylglyoxal (C$_3$H$_4$O$_2$H$^+$, *m/z* = 73.03), 2-butanol (C$_4$H$_{10}$OH$^+$ *m/z* = 75.08), formaldehyde (CH$_2$OH$^+$ *m/z* = 31.02), ketene (C$_2$H$_2$OH$^+$, *m/z* = 43.02), methanol (CH$_4$OH$^+$, *m/z* = 33.03), 2-methylbutanoic acid (C$_5$H$_{10}$O$_2$H$^+$, *m/z* = 103.07), and propanal (C$_3$H$_6$OH$^+$, *m/z* = 59.05). All the products observed by GC-MS and FTIR, except CO and HCl, were also observed by PTR-ToF-MS. In the PTR-ToF-MS analysis, it was observed that 2MB yields two different ions when ionized: C$_5$H$_{10}$OH$^+$ (39%) and C$_2$H$_4$OH$^+$ (61%). As the most abundant fragment from 2MB, C$_2$H$_4$OH$^+$, overlaps with the molecular ion from acetaldehyde, in order to quantify this product the contribution of 2MB to the C$_2$H$_4$OH$^+$ signal was eliminated taking into account its correlation with the C$_5$H$_{10}$OH$^+$ signal when only 2MB was present in the chamber. In **Fig. 8** the time-evolution of 2MB (plotted as the sum of the two identified ions) and the main products, acetaldehyde, butanone, and methylglyoxal, are shown. The molar product yields, obtained from the plots shown in **Fig. S9b**, were (67.9±0.8)%, (34.9±0.6)%, and (14.8±0.2)%, respectively. In addition, very low concentrations of 2-butanol were detected with a product yield of (0.11±0.03)%. It must be noted that formaldehyde and ketene are formed during UV light exposure of 2-methylbutanal in the test prior the Cl reaction, but at very low concentrations (<7.38×10^{10} molecules cm^{-3}) compared with the observed levels after the Cl reaction.
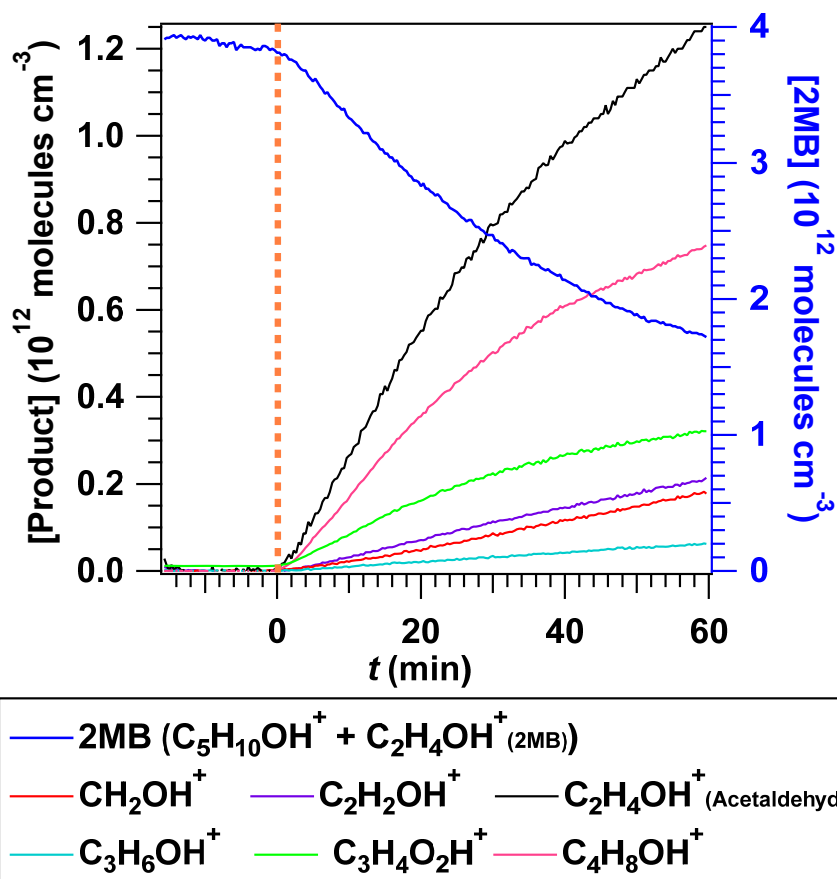
370 **Figure 8.** Temporal evolution of 2-methylbutanal (sum of the 2 identified ions) and the most abundant products measured by PTR-ToF-MS during the 2-methylbutanal + Cl reaction. Vertical dashed line indicates when UV lamps are switched on.

3.3.3 Secondary Organic Aerosols (SOAs).

The yield of SOAs formed in the Cl+2MB reaction, Y_{SOA}, was determined under different conditions (see **Table S3)** from plots such as the presented in **Fig. S11**. As summarized in **Table S3,** Y_{SOA} ranged from 0.16 % to 0.76 % and shows a negative dependence on $[2MB]_0/[Cl_2]_0$, *i.e.* it decreased when that ratio increased. The size distribution of the particles formed in the Cl+2MB reaction with diameters (D_p) between 6 and 523 nm is shown in **Fig. S12** in terms of the normalized particle number, $d\mathrm{N}/d\mathrm{log}D_p$, and mass, $d\mathrm{M}/d\mathrm{log}D_p$. The maximum $d\mathrm{M}/d\mathrm{log}D_p$ was observed at diameters near 500 nm, close to the maximum D_p that the FMPS apparatus can measure. After 12-30 min of reaction, SOAs coagulated ($D_p>500$ nm), not being able to be detected by the FMPS.

3.4 Photodegradation mechanisms

3.4.1 Mechanism of the UV photodissociation of 2MB

It is clear that the molecular elimination of CO (channel (R1c)) occurs since butane (Y_{butane}=9.80%) and CO were detected. Although CO is directly produced in channel (R1c), it can also be rapidly produced by reaction of formyl radical, HCO, formed in channel (R1b), with O_2 (**Figure S13b**). Butanone ($Y_{butanone}$=14.8%) is plausible to be formed from the radical forming channels (R1a) and (R1b). The $CH_3CH_2CH(CH_3)CO$ and $CH_3CH_2CH(CH_3)$ radicals formed in those reactions, respectively, react rapidly with O_2 to produce the corresponding peroxy (RO_2) radical that is involved in a sequence of reactions to generate butanone, among other species. Other molecular photolysis pathways are (Gruver and Calvert, 1956; Wenger, 2006):

$$CH_3CH_2CH(CH_3)C(O)H + h\upsilon \rightarrow CH_4 + CH_3CH=CHC(O)H \qquad (R1d)$$

$$\rightarrow CH_2=CH_2 + CH_3CH=CHOH \qquad (R1e)$$

None of these products were detected by PTR-ToF-MS or GC-MS. However, it is possible that $CH_3CH=CHC(O)H$ and/or $CH_3CH=CHOH$, were responsible of the remaining bands observed in the residual IR spectrum although this could not be justified due to the lack of reference spectra. Neither CH_4 nor $CH_2=CH_2$ could be clearly detected.

3.4.2 Mechanism of the 2MB + Cl reaction

After evaluating the gas-phase products formed in the Cl-reaction with 2-methylbutanal, some information can be inferred concerning the reaction mechanism. The presence of HCl as a primary product and the fact that no other chlorinated products were observed indicate that the reaction proceeds *via* the H-abstraction from different sites in 2MB. There are five susceptible reaction sites in 2MB:

$$Cl + CH_3CH_2CH(CH_3)C(O)H \rightarrow CH_3CH_2CH(CH_3)C(O) + HCl \tag{R3a}$$
$$\rightarrow CH_3CH_2C(CH_3)C(O)H + HCl \tag{R3b}$$
$$\rightarrow CH_3CHCH(CH_3)C(O)H + HCl \tag{R3c}$$
$$\rightarrow CH_2CH_2CH(CH_3)C(O)H + HCl \tag{R3d}$$
$$\rightarrow CH_3CH_2CH(CH_2)C(O)H + HCl \tag{R3e}$$

The mechanism for the H-abstraction from the -C(O)H group and from the hydrocarbon chain are depicted in **Fig. S13a and Fig. S14**, respectively. As shown in the figures, acetaldehyde ($CH_3C(O)H$), formaldehyde ($HC(O)H$) or methanol (CH_3OH) formation can be explained by any of the 5 possibilities, $CH_3CH_2C(O)CH_3$ can be only formed if the aldehydic H (**Figure S13a**) or the tertiary H in C-2 are abstracted (**Figure S14a**), and methylglyoxal ($CH_3C(O)C(O)H$) is a product only when a hydrogen atom from C-2 and C-3 is abstracted (**Figure S14a-b**). Although abstraction at the –C(O)H and tertiary C-2 site are likely dominant, methylglyoxal may not be a major product of C-3 and thus our product data are not conclusive on this issue.

4. Atmospheric implications

Considering the most important diurnal degradation pathways (UV photolysis and reactions with OH radicals and Cl atoms), the relative importance of these three degradation routes on the total atmospheric loss of 2MB, k_{atmos_loss}(2MB), can be estimated, according to Eq(7).

$$k_{atmos\_loss}(2MB) = J(z,\theta) + k_{OH}[OH] + k_{Cl}[Cl] \tag{7}$$

where $J(z,\theta)$ is the photolysis rate of 2MB at a certain altitude z and zenith solar angle (θ); k_{OH} and k_{Cl} are those determined in this work at 298 K; and [OH] and [Cl] are the tropospheric concentrations of OH radicals and Cl atoms, which depend on the considered scenario. Each term was estimated for a coastal city (Valencia, Spain) at sea level (z=0 km) for two scenarios: (*i*) as a function of time from 6:00 to 18:00 LT (local time, corresponding to GMT+2) and (*ii*) for 24-h average conditions. $J(z,\theta)$ is defined as follows (Jiménez et al., 2007):

$$J(z,\theta) \cong \Phi_{eff} \sum_{\lambda>290nm} F(\lambda,z,\theta)\sigma_\lambda \Delta\lambda \tag{8}$$

σ_λ used in the calculation were those listed in **Table S1** and Φ_{eff} = 0.30, determined in this work. $F(\lambda,z,\theta)$ (in photons cm^{-2} nm^{-1} s^{-1}) is the solar spectral actinic flux at 0 km for a specific θ in the troposphere, obtained using the TUV radiative transfer model (5.3 version) developed by Madronich and Flocke (1999) and $\Delta\lambda$ = 1 nm. In scenario (*i*), $F(\lambda,z,\theta)$ was set for θ between 16° at 14:00 LT and 96° at 6:00 LT, while in scenario (*ii*) $F(\lambda,z,\theta)$ is the 24-h average solar spectral actinic flux. The estimated $J(z,\theta)$ values at sea level as a function of the zenith angle are provided in **Table 5**. As expected, it is observed that photolysis is faster at 14:00 ($J(z,\theta)$ = 2.90×10^{-5} s^{-1}) when the solar actinic flux is maximum, whereas it is negligible at the beginning and the end of the day. In scenario (*ii*), the calculated $J(z,\theta)$ was 9.84×10^{-6} s^{-1}.

Table 5. Estimated photolysis rate coefficients of 2-methylbutanal at sea level ($z = 0$ km) in the summer solstice day in Valencia (Spain).

Local time (GMT+2)	θ (°)	$J(z,\theta)$ (10^{-5} s^{-1})
6:00	96	~ 0
8:00	76	0.356
10:00	53	1.51
12:00	31	2.51
14:00	16	2.90
16:00	29	2.55
18:00	52	1.57

435   To calculate the contribution of the OH-reaction to k_{atmos_loss}(2MB) in scenario (*i*), the temporal values of [OH] are considered to be similar to those modelled by Forberich et al. (1999) for a day at the end of June at Weybourne (UK), location with similar θ than Valencia in June, except for the central time of the day. In scenario (*ii*) a 24 h-average of 1×10^6 radicals cm^{-3} (Krol et al., 1998) was accepted for [OH]. In contrast, [Cl] was considered as a time-independent value in both scenarios. In scenario (*i*) an upper limit of 1.3×10^5 atoms cm^{-3}, taken as the peak Cl concentration predicted by Spicer et al. (1998) in

440   marine environments, was considered, while a 24 h-average value of 1×10^3 atoms cm^{-3} (Singh et al., 1996) was assumed in scenario (*ii*).

Taking into account all these calculations, the relative contribution of each degradation route evaluated in this study to the diurnal loss of 2MB in scenario (*i*) is depicted in **Fig. 9**. At dawn, the Cl-reaction dominates the loss of 2MB with a relative contribution of 84%, followed by the OH-reaction (16%). On the other hand, in the central times of the day, OH-

445   reaction is clearly the main removal route for 2MB, with a relative contribution of 79% at 14:00, followed by a competition between photolysis (11%) and Cl-reaction (10%). Note that the relative contribution of Cl-reaction is an upper limit as the considered [Cl] is a peak value. In scenario (*ii*), the OH-reaction is the main removal route for 2MB with a relative contribution of 72.7%, followed by UV photolysis (26.7%). The relative contribution of the Cl-reaction is very small (0.6%), which seems to be more realistic than using the peak Cl concentration.

450
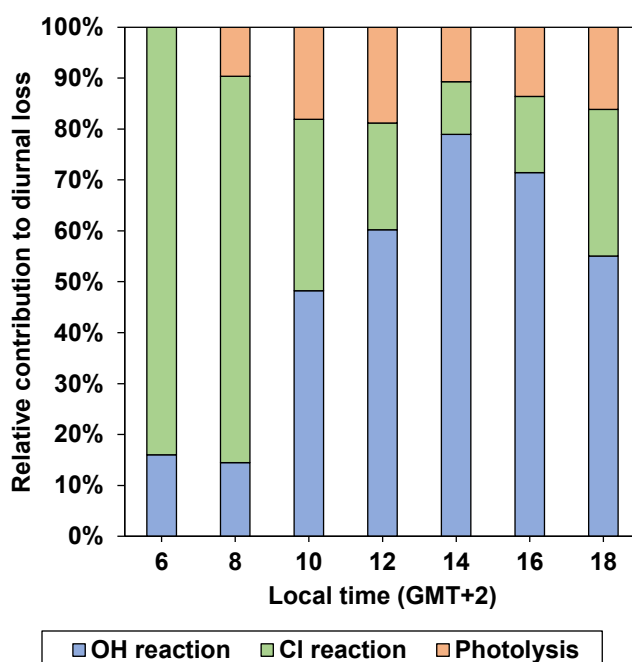
Figure 9. Relative contribution of the three removal routes studied in this work to the total diurnal loss.

The tropospheric lifetime of 2MB, τ, can be estimated according to Eq. (9) using the conditions of scenario (*ii*).

$$\frac{1}{\tau} = \frac{1}{J(z,\theta)} + \frac{1}{k_{OH}[OH]} + \frac{1}{k_{Cl}[Cl]} \tag{9}$$

In the atmosphere of Valencia (Spain) in June, the overall τ for 2MB was estimated to be 7.5 h. Once emitted, 2MB is degraded

in few hours during daytime, so it will not be transported to long distances. Its degradation products include CO and carbonyl compounds such as butanone, acetaldehyde, or methylglyoxal, that can be further oxidized in the troposphere and contribute to photochemical smog, impacting on human health. The evidence found in this work shows that ultrafine particles are formed in the Cl+2MB reaction, but with yields of less than 1%. Therefore, little impact on human health is expected by inhalation at those concentration levels. Finally, HCl, detected in the oxidation of 2MB by Cl, can contribute to acid rain.-However, it must be noted that the impact of the observed products on air quality and human health has a strong dependence on the amounts of

2MB emitted to the troposphere.

5. Conclusions

This work presents a comprehensive study on the relative importance of the most important diurnal atmospheric degradation routes of 2-methylbutanal (2MB) and on the formation of secondary pollutants (particulate matter and gaseous products). This

study describes, for the first time, the kinetics of the UV photolysis of 2MB at (298 ± 2) K and (760 ± 3) Torr, the temperature dependence of the rate coefficient for the OH+2MB reaction between 263 and 353 K at $P_T = 50\text{-}600$ Torr of He, and the rate coefficient of the Cl+2MB reaction at 298 K and 760 Torr. For the summer solstice day in Valencia (Spain), it was found that, on 24-h average, the OH-reaction is the main removal route for 2MB, with a relative contribution of ca. 73%. UV photolysis of 2MB is also important, corresponding to a ca. 27% of its total diurnal loss. Under these conditions, the overall tropospheric

lifetime for 2MB was estimated to be 7.5 h. In terms of the degradation products, it must be noted that the conditions used in this work ($[RO_2]>[HO_2]$) cannot be directly extrapolated to a real clean atmosphere, where the HO_2 reactions are more important than those for RO_2 radicals. However, the end-products identified in this work (CO, HCl, butanone, acetaldehyde, and methylglyoxal) are expected to be the same. Major products of the Cl+2MB reaction are butanone, acetaldehyde, CO and HCl, but methylglyoxal was also detected. UV photolysis of 2MB in the actinic region produces butane, butanone, and CO as

major products. The carbonyl products formed can contribute to photochemical smog, whereas HCl can contribute to acid rain, however the real impact of will depend on the amounts of 2MB emitted to the troposphere. In addition, the yield of secondary organic aerosols formed in the Cl+2MB reaction is too small (<1%) to affect the human health.

Author contribution

M. As., M. An., and S. B. designed and conducted the experiments, and analysed the experimental data. E.J. and J.A. designed and supervised the experiments and managed the project. All the co-authors have contributed to prepare the manuscript and to discuss the obtained results.

Acknowledgements

490 This work has been supported by the Regional government of Castilla-La Mancha through CINEMOL project (Ref.: SBPLY/19/180501/000052) and by the University of Castilla-La Mancha – UCLM (*Ayudas para la financiación de actividades de investigación dirigidas a grupos* (REF: 2019-GRIN-27175). M. Asensio, M. Antiñolo and S. Blázquez also acknowledge UCLM (*Plan Propio de Investigación*) for funding their contracts during the performance of this investigation.

Electronic Supplementary Information

The electronic supplementary information includes additional tables, figures, and description of the methods. In addition, the SI also includes an Excel file with the determined UV and IR absorption cross sections as a function of wavelength.

500

References

Albaladejo, J., Ballesteros, B., Jiménez, E., Martín, P., and Martínez, E.: A PLP–LIF kinetic study of the atmospheric reactivity of a series of C4–C7 saturated and unsaturated aliphatic aldehydes with OH, Atmospheric Environment, 36, 3231-3239, https://doi.org/10.1016/S1352-2310(02)00323-0, 2002.

Antiñolo, M., Asensio, M., Albaladejo, J., and Jiménez, E.: Gas-Phase Reaction of trans-2-Methyl-2-butenal with Cl: Kinetics, Gaseous Products, and SOA Formation, Atmosphere, 11, 715, https://doi.org/10.3390/atmos11070715, 2020.

Antiñolo, M., Jiménez, E., Notario, A., Martínez, E., and Albaladejo, J.: Tropospheric photooxidation of CF_3CH_2CHO and $CF_3(CH_2)_2CHO$ initiated by Cl atoms and OH radicals, Atmospheric Chemistry and Physics, 10, 1911-1922, https://doi.org/10.5194/acp-10-1911-2010, 2010.

Antiñolo, M., Olmo, R. d., Bravo, I., Albaladejo, J., and Jiménez, E.: Tropospheric fate of allyl cyanide (CH_2=$CHCH_2CN$): Kinetics, reaction products and secondary organic aerosol formation, Atmospheric Environment, 219, 117041, https://doi.org/10.1016/j.atmosenv.2019.117041, 2019.

Atkinson, R., Baulch, D. L., Cox, R. A., Crowley, J. N., Hampson, R. F., Hynes, R. G., Jenkin, M. E., Rossi, M. J., Troe, J., and Subcommittee, I.: Evaluated kinetic and photochemical data for atmospheric chemistry: Volume II – gas phase reactions of organic species, Atmospheric Chemistry and Physics, 6, 3625-4055, https://doi.org/10.5194/acp-6-3625-2006, 2006.

Ballesteros, B., Jiménez, E., Moreno, A., Soto, A., Antiñolo, M., and Albaladejo, J.: Atmospheric fate of hydrofluoroolefins, $C_xF_{2x+1}CH$=CH_2 (x = 1,2,3,4 and 6): Kinetics with Cl atoms and products, Chemosphere, 167, 330-343, https://doi.org/10.1016/j.chemosphere.2016.09.156, 2017.

Blázquez, S., González, D., Neeman, E. M., Ballesteros, B., Agúndez, M., Canosa, A., Albaladejo, J., Cernicharo, J., and Jiménez, E.: Gas-phase kinetics of CH_3CHO with OH radicals between 11.7 and 177.5 K, Physical Chemistry Chemical Physics, 22, 20562-20572, https://doi.org/10.1039/D0CP03203D, 2020.

Ceacero-Vega, A. A., Ballesteros, B., Bejan, I., Barnes, I., Jiménez, E., and Albaladejo, J.: Kinetics and Mechanisms of the Tropospheric Reactions of Menthol, Borneol, Fenchol, Camphor, and Fenchone with Hydroxyl Radicals (OH) and Chlorine Atoms (Cl), The Journal of Physical Chemistry A, 116, 4097-4107, https://doi.org/10.1021/jp212076g, 2012.

D'Anna, B., Andresen, Ø., Gefen, Z., and Nielsen, C. J.: Kinetic study of OH and NO_3 radical reactions with 14 aliphatic aldehydes, Physical Chemistry Chemical Physics, 3, 3057-3063, https://doi.org/10.1039/B103623H, 2001.

Flaig, M., Qi, S., Wei, G., Yang, X., and Schieberle, P.: Characterization of the Key Odorants in a High-Grade Chinese Green Tea Beverage (*Camellia sinensis*; *Jingshan cha*) by Means of the Sensomics Approach and Elucidation of Odorant Changes in Tea Leaves Caused by the Tea Manufacturing Process, Journal of Agricultural and Food Chemistry, 68, 5168-5179, https://doi.org/10.1021/acs.jafc.0c01300, 2020.

Forberich, O., Pfeiffer, T., Spiekermann, M., Walter, J., Comes, F. J., Grigonis, R., Clemitshaw, K. C., and Burgess, R. A.: Measurement of the Diurnal Variation of the OH Radical Concentration and Analysis of the Data by Modelling, Journal of Atmospheric Chemistry, 33, 155-181, https://doi.org/10.1023/A:1005973130335, 1999.

Griesser, M., Weingart, G., Schoedl-Hummel, K., Neumann, N., Becker, M., Varmuza, K., Liebner, F., Schuhmacher, R., and Forneck, A.: Severe drought stress is affecting selected primary metabolites, polyphenols, and volatile metabolites in grapevine leaves (*Vitis vinifera* cv. Pinot noir), Plant Physiology and Biochemistry, 88, 17-26, https://doi.org/10.1016/j.plaphy.2015.01.004, 2015.

Gruver, J. T. and Calvert, J. G.: The Vapor Phase Photolysis of 2-Methylbutanal at Wave Length 3130 Å.[1], Journal of the American Chemical Society, 78, 5208-5213, https://doi.org/10.1021/ja01601a021, 1956.

Gueymard, C. A., Myers, D., and Emery, K.: Proposed reference irradiance spectra for solar energy systems testing, Solar Energy, 73, 443-467, https://doi.org/10.1016/S0038-092X(03)00005-7, 2002.

Jiménez, E., Lanza, B., Martínez, E., and Albaladejo, J.: Daytime tropospheric loss of hexanal and *trans*-2-hexenal: OH kinetics and UV photolysis, Atmospheric Chemistry and Physics, 7, 1565-1574, https://doi.org/10.5194/acp-7-1565-2007, 2007.

Kolar, P. and Kastner, J. R.: Low-temperature catalytic oxidation of aldehyde mixtures using wood fly ash: Kinetics, mechanism, and effect of ozone, Chemosphere, 78, 1110-1115, https://doi.org/10.1016/j.chemosphere.2009.12.033, 2010.

545 Krol, M., van Leeuwen, P. J., and Lelieveld, J.: Global OH trend inferred from methylchloroform measurements, J. Geophys. Res. Atmos., 103, 10697-10711, https://doi.org/10.1029/98JD00459, 1998.

Madronich, S. and Flocke, S.: The Role of Solar Radiation in Atmospheric Chemistry, in: Environmental Photochemistry, edited by: Boule, P., Springer Berlin Heidelberg, Berlin, Heidelberg, 1-26, https://doi.org/10.1007/978-3-540-69044-3_1, 1999.

Martínez, E., Albaladejo, J., Jiménez, E., Notario, A., and Aranda, A.: Kinetics of the reaction of CH_3S with NO_2 as a function of temperature,
550 Chemical Physics Letters, 308, 37-44, https://doi.org/10.1016/S0009-2614(99)00579-5, 1999.

Millet, D. B., Guenther, A., Siegel, D. A., Nelson, N. B., Singh, H. B., de Gouw, J. A., Warneke, C., Williams, J., Eerdekens, G., Sinha, V., Karl, T., Flocke, F., Apel, E., Riemer, D. D., Palmer, P. I., and Barkley, M.: Global atmospheric budget of acetaldehyde: 3-D model analysis and constraints from in-situ and satellite observations, Atmos. Chem. Phys., 10, 3405-3425, https://doi.org/10.5194/acp-10-3405-2010, 2010.

555 Orlando, J. J., Tyndall, G. S., Apel, E. C., Riemer, D. D., and Paulson, S. E.: Rate coefficients and mechanisms of the reaction of cl-atoms with a series of unsaturated hydrocarbons under atmospheric conditions, International Journal of Chemical Kinetics, 35, 334-353, https://doi.org/10.1002/kin.10135, 2003.

Singh, H. B., Thakur, A. N., Chen, Y. E., and Kanakidou, M.: Tetrachloroethylene as an indicator of low Cl atom concentrations in the troposphere, Geophysical Research Letters, 23, 1529-1532, https://doi.org/10.1029/96GL01368, 1996.

560 Spicer, C. W., Chapman, E. G., Finlayson-Pitts, B. J., Plastridge, R. A., Hubbe, J. M., Fast, J. D., and Berkowitz, C. M.: Unexpectedly high concentrations of molecular chlorine in coastal air, Nature, 394, 353-356, https://doi.org/10.1038/28584, 1998.

Urbanski, S. P., Hao, W. M., and Baker, S.: Chapter 4 Chemical Composition of Wildland Fire Emissions, in: Developments in Environmental Science, edited by: Bytnerowicz, A., Arbaugh, M. J., Riebau, A. R., and Andersen, C., Elsevier, 79-107, https://doi.org/10.1016/S1474-8177(08)00004-1, 2008.

565 Utrilla-Vázquez, M., Rodríguez-Campos, J., Avendaño-Arazate, C. H., Gschaedler, A., and Lugo-Cervantes, E.: Analysis of volatile compounds of five varieties of Maya cocoa during fermentation and drying processes by Venn diagram and PCA, Food Research International, 129, 108834, https://doi.org/10.1016/j.foodres.2019.108834, 2020.

Wallington, T. J., Ball, J. C., Straccia, A. M., Hurley, M. D., Kaiser, E. W., Dill, M., Schneider, W. F., and Bilde, M.: Kinetics and mechanism of the reaction of Cl atoms with CH_2CO (Ketene), International Journal of Chemical Kinetics, 28, 627-635,
570 https://doi.org/10.1002/(SICI)1097-4601(1996)28:8<627::AID-KIN8>3.0.CO;2-X, 1996.

Wenger, J. C.: Chamber Studies on the Photolysis of Aldehydes Environmental, Dordrecht, 111-119, https://doi.org/10.1007/1-4020-4232-9_8, 2006.